Applied Scientific Research **52:** 115–132, 1994.

On the Universality of the Velocity Profiles of a Turbulent Flow in an Axially Rotating Pipe

B. WEIGAND and H. BEER
Institut für Technische Thermodynamik, Technische Hochschule Darmstadt, Petersenstraße 30, 64287 Darmstadt, Germany

Received 23 June 1992; accepted in revised form 24 October 1992

Abstract. If a fluid enters an axially rotating pipe, it receives a tangential component of velocity from the moving wall, and the flow pattern change according to the rotational speed. A flow relaminarization is set up by an increase in the rotational speed of the pipe. It will be shown that the tangential- and the axial velocity distribution adopt a quite universal shape in the case of fully developed flow for a fixed value of a new defined rotation parameter. By taking into account the universal character of the velocity profiles, a formula is derived for describing the velocity distribution in an axially rotating pipe. The resulting velocity profiles are compared with measurements of Reich [10] and generally good agreement is found.

Nomenclature

b	= constant, equation (34)
D	= pipe diameter
l	= mixing length
l_0	= mixing length in a non-rotating pipe
N	= rotation rate, $N = \mathrm{Re}_\varphi/\mathrm{Re}_D$
p	= pressure
R	= pipe radius
Re_D	= flow-rate Reynolds number, $\mathrm{Re}_D = \bar{v}_z D/\nu$
Re_φ	= rotational Reynolds number, $\mathrm{Re}_\varphi = v_{\varphi w} D/\nu$
Re_*	= Reynolds number based on the friction velocity, $\mathrm{Re}_* = v_* R/\nu$
$(\mathrm{Re}_*)_0$	= Reynolds number based on the friction velocity in a non-rotating pipe
Ri	= Richardson number, equation (10)
r	= coordinate in radial direction
$\tilde{r}$	= dimensionless coordinate in radial direction, $\tilde{r} = r/R$
v_r, v_φ, v_z	= time mean velocity components
v_r', v_φ', v_z'	= velocity fluctations
$v_{\varphi w}$	= tangential velocity of the pipe wall
v_*	= friction velocity, $v_* = \sqrt{\lvert\tau_{rz}\rvert_w/\rho}$
$\bar{v}_z$	= axial mean velocity
v_{ZM}	= maximum axial velocity
$\tilde{y}$	= dimensionless radial distance from pipe wall, $\tilde{y} = 1 - \tilde{r}$
y^+	= dimensionless radial distance from pipe wall
y_1^+	= constant
Z	= rotation parameter, $Z = v_{\varphi w}/v_* = N\ \mathrm{Re}_D/2\mathrm{Re}_*$
ε_m	= eddy viscosity
$(\varepsilon_m)_0$	= eddy viscosity in a non-rotating pipe
λ	= coefficient of friction loss
κ	= von Karman constant

κ_1 = constant, equation (31)
ρ = density
μ = dynamic viscosity
ν = kinematic viscosity

1. Introduction

Fluid flow and heat transfer in rotating systems are not only of considerable theoretical interest, but also of great practical importance. Transport phenomena in rotating systems, therefore, have challenged engineers and scientists for a long time. In 1917 Lord Rayleigh [8] investigated the dynamcis and stability of revolving fluids. Also, some of the classical solutions of the Navier-Stokes equations were obtained for rotating systems. Von Kármán [3] investigated the flow induced by a rotating disk and the associated convective heat transfer in 1921. The fluid mechanics stability criteria for circular flow in an annulus formed between two concentric rotating cylinders were studied by Taylor [13]. Another rather elementary and common rotating configuration, which is the subject of this paper, is the case of flow through a rotating pipe. The obvious technical application is a rotating power transmission shaft that is longitudinally bored, and through which a fluid is pumped for cooling or for other purposes.

When a fluid enters a pipe rotating about its axis, tangential forces acting between the rotating pipe and the fluid cause the fluid to rotate with the pipe, resulting in a flow pattern rather different from that observed in a non-rotating pipe. Rotation was found to have a very marked influence on the suppression of the turbulent motion because of radially growing centrifugal forces. The effects of pipe rotation on the hydraulic loss have been investigated experimentally by Levy [6], White [15] and Shchukin [12]. If the flow is initially turbulent, the pressure loss decreases with increasing rotational speed. For turbulent flows in a rotating pipe, Borisenko et al. [1] studied the effect of rotation on the turbulent velocity fluctuations using hot-wire probes and showed that they were suppressed by the rotation. Murakami and Kikuyama [7] measured the time-mean velocity components and hydraulic losses in an axially rotating pipe when a fully developed turbulent flow was introduced into the pipe. The pipe rotation was found to suppress the turbulence in the flow, and also to reduce the hydraulic loss. With increasing rotational speed, the axial velocity distribution finally approaches the Hagen-Poiseuille flow. By using a modified mixing length theory for the turbulent pipe flow, Kikuyama et al. [4] calculated velocity distributions and friction coefficients in the fully developed region of a rotating pipe. They found that a flow relaminarization was set up by an increase in the rotational speed of the pipe, if the flow in the pipe is initially turbulent. Additional experiments confirmed the results of the calculations. Reich and Beer [10] calculated the velocity distribution and the heat transfer in an axially rotating pipe for the case of fully developed flow. They used a mixing length model which was slightly altered as the one given in [4]. Hirai and Takagi [2] were able to

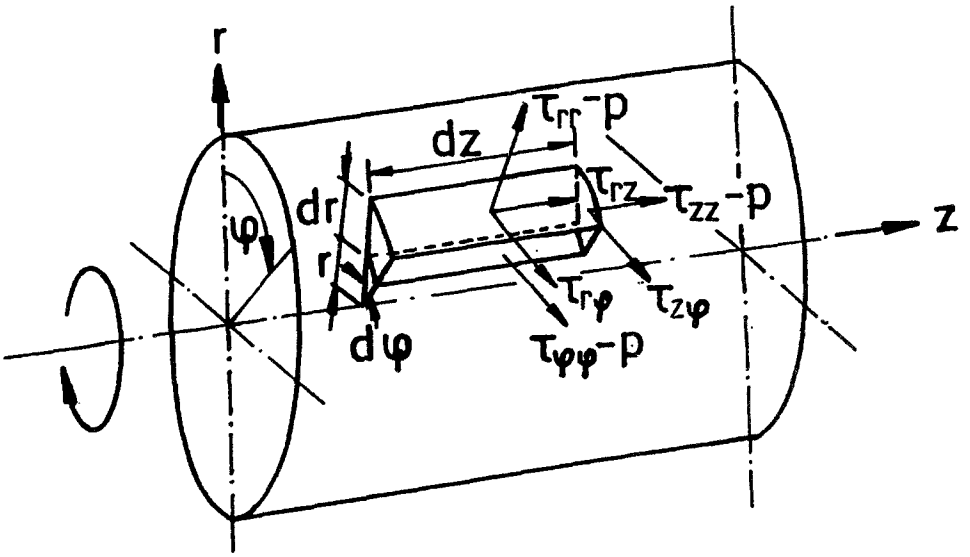

Fig. 1. Coordinate system.

predict the velocity and temperature distribution in an axially rotating pipe for fully developed flow conditions with the help of a Reynolds stress turbulence model. In this case there was no necessity to assume the tangential velocity distribution as it was done in [4] and [10].

The following study will focus attention on the universal character of the velocity distribution in an axially rotating pipe. A complete representation of the velocity distribution is derived for fully developed flow.

2. Analysis

Figure 1 shows the physical model and the coordinate system. By assuming fully developed flow conditions, rotational symmetry and an incompressible Newtonian fluid with constant fluid properties, the conservation equations in cylindrical coordinates adopt the following form

$$-\rho\frac{v_\varphi^2}{r} = -\frac{\partial p}{\partial r} - \frac{\rho}{r}\frac{\partial}{\partial r}\left(r\overline{v_r' v_r'}\right) + \rho\frac{\overline{v_\varphi' v_\varphi'}}{r} \tag{1}$$

$$0 = \frac{1}{r^2}\frac{\partial}{\partial r}\left(\mu r^3\frac{\partial}{\partial r}\left(\frac{v_\varphi}{r}\right) - \rho r^2\overline{v_r' v_\varphi'}\right) \tag{2}$$

$$0 = -\frac{\partial p}{\partial z} + \frac{1}{r}\frac{\partial}{\partial r}\left(\mu r\frac{\partial v_z}{\partial r} - \rho r\overline{v_r' v_z'}\right) \tag{3}$$

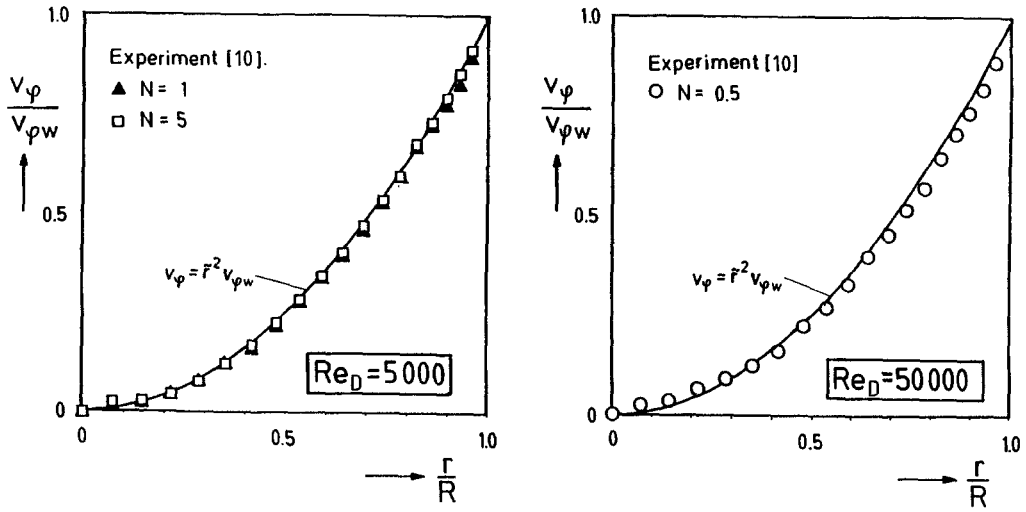

Fig. 2. Tangential velocity distribution.

The boundary conditions belonging to equations (1)–(3) are

$$r = R : v_\varphi = v_{\varphi w}, \quad v_r = 0, \quad v_z = 0$$

$$r = 0 : v_\varphi = 0, \quad v_r = 0, \quad \frac{\partial v_z}{\partial r} = 0. \tag{4}$$

Because the flow is fully developed, the radial component of the time-mean velocity must be zero. According to experiments in references [4], [7], [10], the tangential velocity profile in the fully developed region was found to be universal. The tangential velocity distribution can be characterized by a parabolic distribution

$$v_\varphi = v_{\varphi w} \left(\frac{r}{R}\right)^2 \tag{5}$$

Figure 2 shows a comparison between the approximation according to equation (5) and measurements performed by Reich [10]. It can be seen that the tangential velocity distribution, scaled wih the velocity of the pipe wall, is neither a function of the flow-rate Reynolds number, nor a function of the rotational speed. Because the tangential velocity distribution is known and the pressure is not a function of the tangential coordinate, the conservation equation in the tangential direction can be ignored.

The axial velocity distribution can be calculated as follows. The axial turbulent shear stress, which appears in equation (3), can be expressed by the time-mean quantities by using a modified mixing length theory as proposed by Koosinlin et al. [5]. This results in the following expression for

$$-\rho \overline{v_r' v_z'} = \rho l^2 \left[\left(\frac{\partial v_z}{\partial r}\right)^2 + \left(r \frac{\partial}{\partial r}\left(\frac{v_\varphi}{r}\right)\right)^2\right]^{1/2} \frac{\partial v_z}{\partial r} = \rho \varepsilon_m \frac{\partial v_z}{\partial r} \tag{6}$$

where l denotes the mixing length

$$\frac{l}{l_0} = \left(1 - \frac{1}{6}\mathrm{Ri}\right)^2 \tag{7}$$

as proposed by Reich and Beer [10]. The mixing length l_0 for a non-rotating pipe flow, which appears in equation (7), can be described by the well-known mixing length formula of Nikuradse, modified with the damping factor of van Driest

$$\frac{l_0}{R} = \left[0.14 - 0.08\left(\frac{r}{R}\right)^2 - 0.06\left(\frac{r}{R}\right)^4\right]\left[1 - \mathrm{e}^{-y^+/26}\right]. \tag{8}$$

Herein y^+ is the dimensionless distance from the wall, defined as

$$y^+ = \frac{v_*(R-r)}{\nu} \tag{9}$$

The Richardson number in equation (7) describes the effect of pipe rotation on the turbulent motion and is defined as

$$\mathrm{Ri} = \frac{2\frac{v_\varphi}{r^2}\frac{\partial}{\partial r}(v_\varphi r)}{\left(\frac{\partial v_z}{\partial r}\right)^2 + \left(r + \frac{\partial}{\partial r}\left(\frac{v_\varphi}{r}\right)\right)^2}. \tag{10}$$

Without rotation, Ri = 0, there exists a fully developed turbulent pipe flow. If Ri > 0, i.e. for a rotating tube with a radially growing tangential velocity, the centrifugal forces suppress the turbulent fluctuations and the mixing length decreases. Inserting equations (6)–(10) into the conservation equation in the axial direction, equation (3) can be cast in the following form

$$0 = \tilde{l}^2\left[\left(\frac{\mathrm{d}\tilde{v}_z}{\mathrm{d}\tilde{r}}\right)^2 + \left(\tilde{r}N\frac{\mathrm{Re}_D}{2\mathrm{Re}_*}\right)^2\right]^{1/2}\frac{\mathrm{d}\tilde{v}_z}{\mathrm{d}\tilde{r}} + \frac{1}{\mathrm{Re}_*}\frac{\mathrm{d}\tilde{v}_z}{\mathrm{d}\tilde{r}} + \tilde{r} \tag{11}$$

with the dimensionless quantities

$$\tilde{l} = l/R, \quad \tilde{r} = r/R, \quad \tilde{v}_z = v_z/v_*, \quad N = \mathrm{Re}_\varphi/\mathrm{Re}_D$$

$$\mathrm{Re}_D = \frac{\bar{v}_z D}{\nu}, \quad \mathrm{Re}_\varphi = \frac{v_{\varphi w} D}{\nu}, \quad \mathrm{Re}_* = \frac{v_* R}{\nu}. \tag{12}$$

In equation (11), the partial differentials were replaced by ordinal differentials, because the velocity $\tilde{v}_z$ is only a function of the radial coordinate $\tilde{r}$. All the studies done in the past concerning turbulent flow in an axially rotating pipe used the quantity N for describing the effect of tube rotation upon the turbulent motion [4], [10]. Therefore, a universal character of the axial velocity profile could not be observed. By examining equation (11), the only parameter which involves the effect of tube rotation on the axial velocity is found to be

$$Z = N\frac{\mathrm{Re}_D}{2\mathrm{Re}_*} = \frac{v_{\varphi w}}{v_*} = N\Big/\sqrt{\frac{\lambda}{8}}. \tag{13}$$

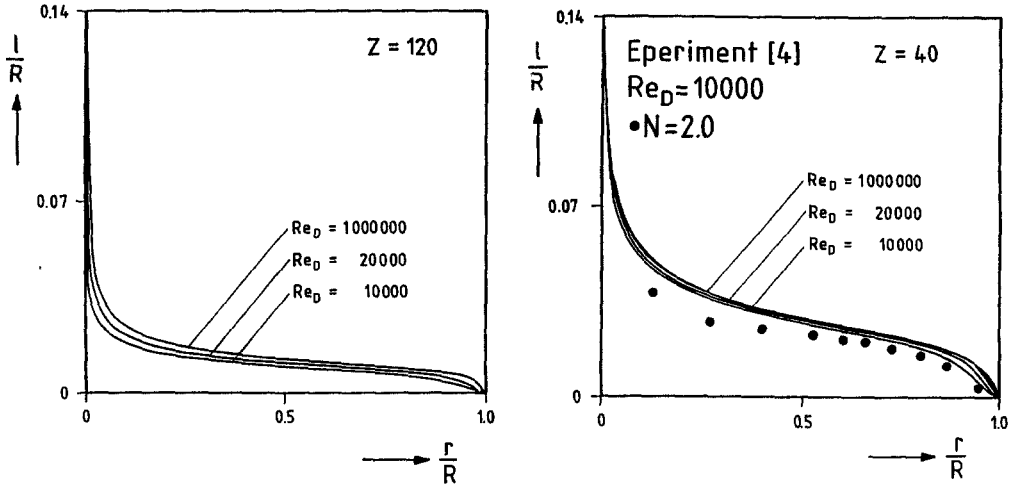

Fig. 3. Mixing length distributions for different values of the flow-rate Reynolds number.

From equation (13) it can be seen that the parameter Z involves the rotation rate N and, further, the coefficient of friction loss λ. The rotation rate N is the ratio of the rotational Reynolds number and the flow-rate Reynolds number as shown in equation (12). N characterizes the effect of rotation on the axial mean velocity in the rotating pipe. The term $\sqrt{\lambda/8}$ takes into account the variation in the shape of the axial velocity profile at the pipe wall and, therefore, includes the effect of different pressure losses in the rotational pipe section due to rotation.

Keeping this fact in mind, one can hope to find a universal axial velocity profile for the flow in an axially rotating pipe, if it can be shown that the mixing length distribution $\tilde{l}$ is not a function of the flow-rate Reynolds number. By inserting equation (5) into the definition of the Richardson number, one obtains

$$\mathrm{Ri} = \frac{6\tilde{r}^2 Z^2}{\left(\frac{\mathrm{d}\tilde{v}_z}{\mathrm{d}\tilde{r}}\right)^2 + \tilde{r}^2 Z^2}. \tag{14}$$

Therefore, the mixing length distribution is only affected by the parameter Z. This fact is elucidated in Figure 3, where the mixing length distribution is plotted for constant values of Z and different flow-rate Reynolds numbers. In Figure 4, the axial velocity distribution is ploted for various values of the rotation parameter Z. The curves presented in Figure 3 and Figure 4 were obtained by solving equation (11) numerically, according to the given boundary conditions. Additionally, a constant flow-rate was required by performing the numerical calculations. It is obvious, that the axial velocity distribution, plotted in the form $(v_{ZM} - v_Z)/v_*$ versus $\tilde{r}$, is not or only a very weak function of the flow rate Reynolds number for a constant value of Z. The case $Z = 0$ represents the flow in a non-rotating pipe.

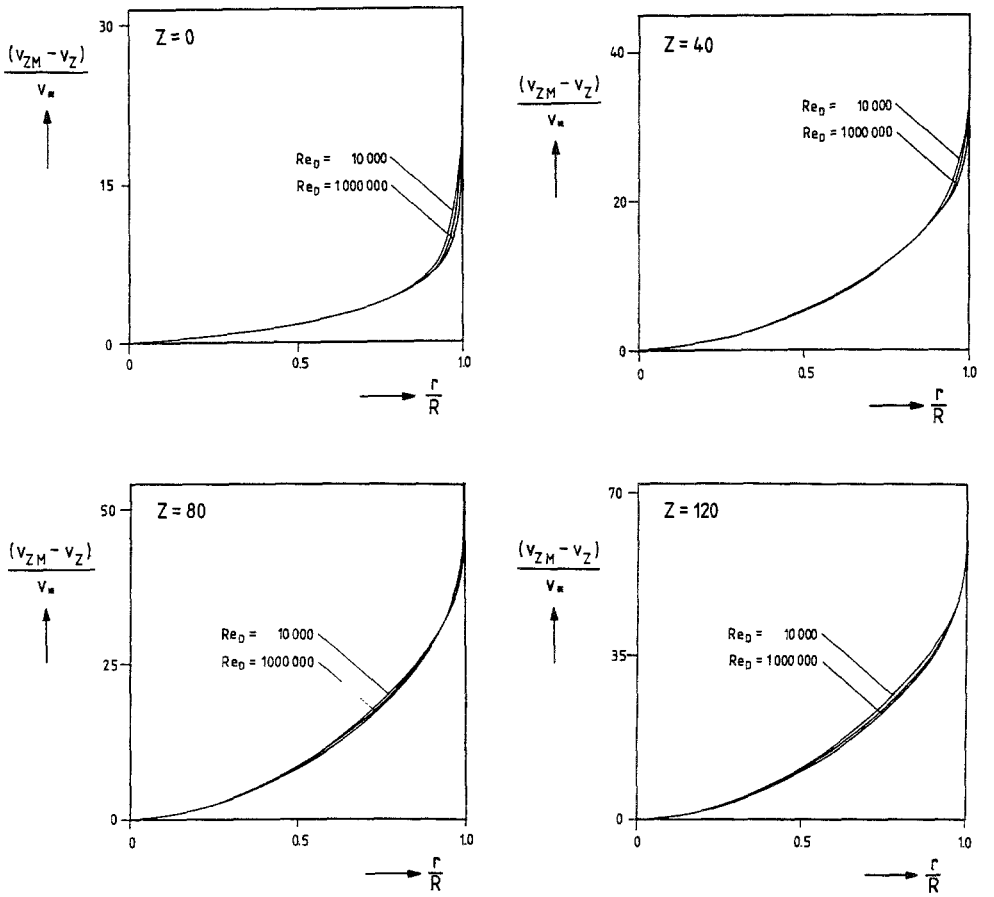

Fig. 4. Axial velocity profiles for various values of the rotation parameter Z and different Re_D.

The rotation parameter Z depends on the rotation rate N and on the flow-rate Reynolds number Re_D. This fact is elucidated in Figure 5. It can be seen that Z = const. demands decreasing values of N for growing flow-rate Reynolds numbers. In Figure 4, it can be observed that the velocity profiles are affected by the flow-rate Reynolds number in the vicinity of the rotating wall of the pipe. This is due to the growing viscous forces in the near wall region.

It is common in the theoretical treatment of non-rotating turbulent pipe flow to split off the flow region into a core region and into a near wall region [11]. In doing so, we will follow the excellent paper of Reichard [9], who developed an approximation formula for the axial velocity profile for a non-rotating turbulent pipe flow.

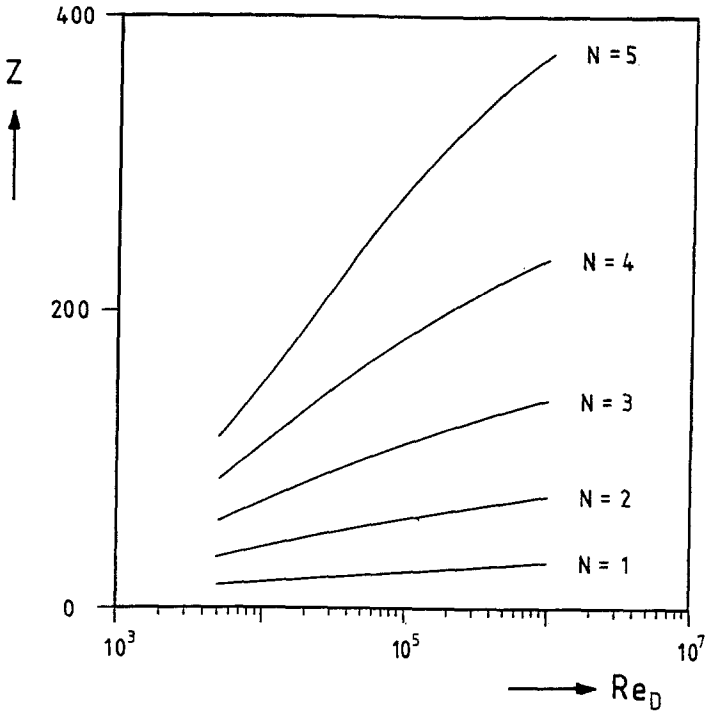

Fig. 5. Rotation parameter Z as a function of the flow-rate Reynolds number with N as parameter.

2.1. The Core Region

By examining equation (11) it is obvious that the term proportional to Re_*^{-1} can be ignored in the core region of the pipe if Re_* becomes large. Figure 6 shows $(v_{ZM} - v_Z)/v_*$ for two different values of Z. It can be seen that the curves are straight lines in the logarithmic diagram in the core region. Therefore, the velocity profiles can be approximated with good accuracy by

$$\frac{v_{ZM} - v_Z}{v_*} = A\tilde{r}^B \tag{15}$$

where the constants A and B are functions of the rotation parameter Z. The functional dependence of A and B on Z can be described by the following equations

$$A(Z) = \sqrt{6.052 \times 10^{-2} Z^2 + 5.4Z + 25.705} \tag{16}$$

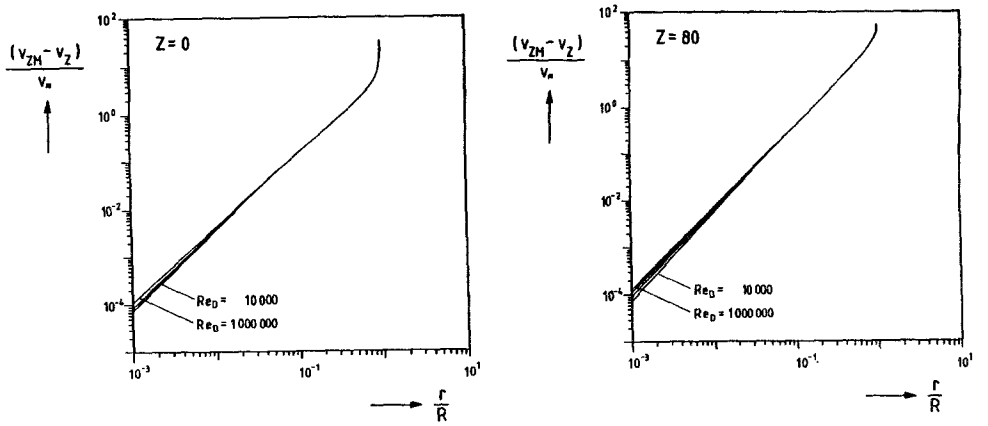

Fig. 6. Axial velocity profiles for $Z = 0$ and $Z = 80$ and various values of Re_D.

$$B(Z) = 1.55 + 0.338[1 - \exp(-5.53 \times 10^{-2} Z)]. \tag{17}$$

For $Z = 0$ the velocity distribution given by equations (15)–(17) reduces to the well known approximation of Darcy [11] for the velocity profile of a turbulent flow in a non-rotating pipe. Figure 7 shows a comparison between the approximation, according to the equations (15)–(17), and numerically predicted velocity profiles. It is obvious that the agreement between both is good for $\tilde{r} < 0.7$. For values of the radial coordinate $\tilde{r} > 0.7$, the approximation deviates from the numerical result, which is due to the more pronounced influence of viscous forces on the shape of the velocity profile. By using equation (15) for calculating the velocity profile, the dependence of v_{ZM} on the rotation parameter Z and on the flow-rate Reynolds number has to be known. Figure 8 shows the variation of v_{ZM}, scaled with the friction velocity v_*, for various values of the rotation parameter Z. It can be seen that v_{ZM}/v_* increases with growing values of Z and with growing values of the flow-rate Reynolds number.

2.2. The Wall Region

Back to Ludwig Prandtl [14] it is known that the velocity profile in the near wall region of a non-rotating pipe can be described by

$$\frac{v_Z}{v_*} = \frac{1}{\kappa} \ln y^+ + 5.5, \tag{18}$$

where $\kappa = 0.4$ is the von Kármán constant. The velocity profiles in the near wall region in a rotating pipe behave quite different than it might be expected from equation (18). Figure 9 shows axial velocity profiles for two different values of Z. It is apparent that the shape of the velocity profiles is strongly disturbed in the near wall region with increasing values of the rotation parameter Z. The region

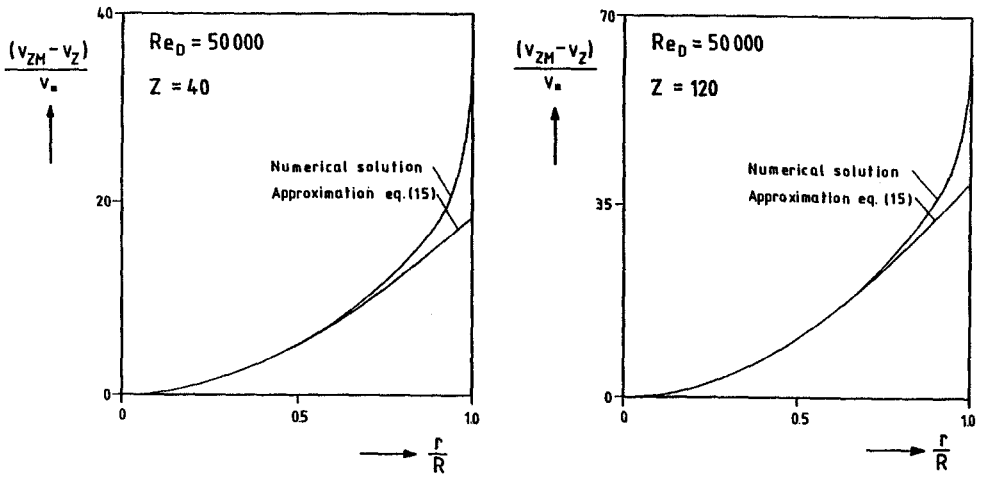

Fig. 7. Comparison between numerical solution and the approximation for the axial velocity distribution in the core region.

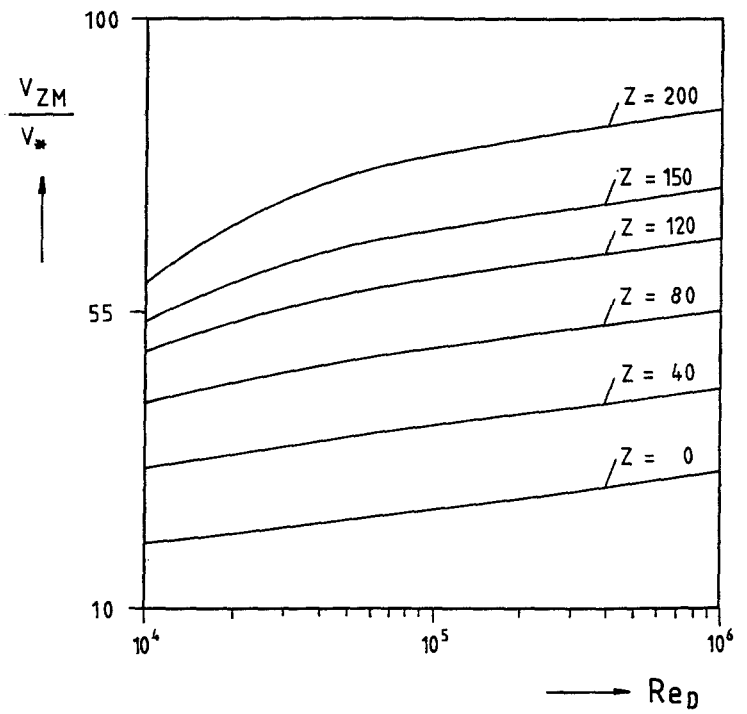

Fig. 8. v_{ZM}/v_* as a function of Re_D for various values of the rotation parameter Z.

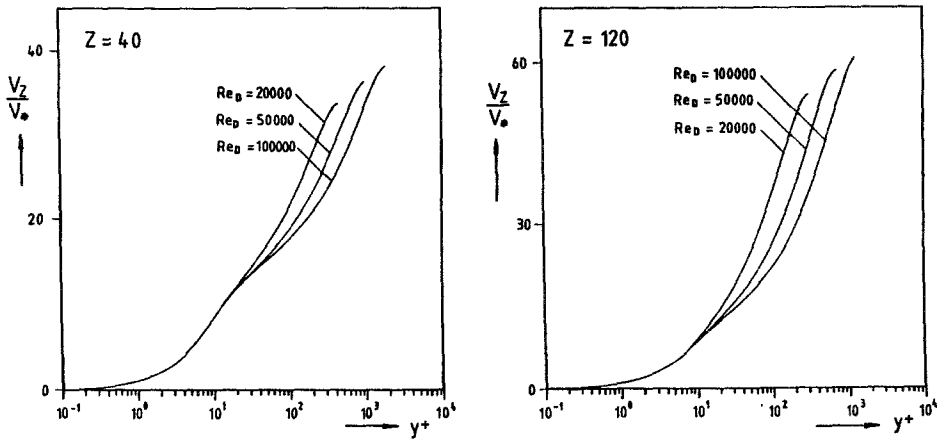

Fig. 9. Axial velocity distribution v_Z/v_* as a function of the wall coordinate y^+ for two different values of Z.

for which a logarithmic shape of the velocity profiles can be observed tends to zero with growing values of Z. This fact can be easily understood by examining equation (11) for $Z \to \infty$. In this case the mixing length tends to zero and the velocity profile is expressed by

$$\frac{v_Z}{v_*} = y^+ - \frac{1}{2}\frac{y^{+2}}{\mathrm{Re}_*} \tag{19}$$

which is a parabolic distribution.

In order to find an approximation for the velocity profile in the near wall region, it is necessary to examine the variation of the eddy viscosity with increasing rotation parameters Z. The eddy viscosity, defined by equation (6), is given in dimensionless form by

$$\varepsilon_m^* = \mathrm{Re}_*^2 \tilde{l}^2 \left[\left(\frac{\mathrm{d}\tilde{v}_Z}{\mathrm{d}y^+} \right)^2 + \left(1 - \frac{y^+}{\mathrm{Re}_*} \right)^2 \left(\frac{Z}{\mathrm{Re}_*} \right)^2 \right]^{1/2} . \tag{20}$$

The distribution of the mixing length $\tilde{l}$ is given by equation (7). Rewritten in wall coordinates, $\tilde{l}$ adopts the following form

$$\tilde{l} = \tilde{l}_0 \left(\frac{\mathrm{d}\tilde{v}_z}{\mathrm{d}y^+} \right)^4 \Bigg/ \left[\left(\frac{\mathrm{d}\tilde{v}_z}{\mathrm{d}y^+} \right)^2 + \left(1 - \frac{y^+}{\mathrm{Re}_*} \right)^2 \left(\frac{Z}{\mathrm{Re}_*} \right)^2 \right]^2 . \tag{21}$$

Examining equation (20) and equation (21) for $y^+ \to 0$, results in the following expression for ε_m^*

$$\varepsilon_m^* \approx \tilde{l}_0^2 \mathrm{Re}_*^2 \Bigg/ \left[\left(\frac{Z}{\mathrm{Re}_*} \right)^2 + 1 \right]^{3.5} . \tag{22}$$

By deriving equation (22) it was assumed that $\tilde{v}_z = y^+$ in the near wall region. In the case of a non-rotating pipe, equation (22) simplifies to

$$\begin{matrix}(\varepsilon_m^*)_0 \approx \tilde{l}_0^2 (\mathrm{Re}_*)_0^2 \\ y^+ \to 0\end{matrix} \tag{23}$$

where the Reynolds number $(\mathrm{Re}_*)_0$ in a non-rotating pipe can easily be calculated from the Blasius friction formula [11].

$$\mathrm{Re}_* = \sqrt{\frac{0.3164}{32}} \mathrm{Re}_D^{0.875}. \tag{24}$$

The ratio $\varepsilon_m^*/(\varepsilon_m^*)_0$ can be expected to be a measure for the relaminarization due to pipe rotation in the near wall region.

$$\begin{matrix}\frac{\varepsilon_m^*}{(\varepsilon_m^*)_0} \\ y^+ \to 0\end{matrix} = \left(\frac{\mathrm{Re}_*}{(\mathrm{Re}_*)_0}\right)^2 \Big/ \left[\left(\frac{Z}{\mathrm{Re}_*}\right)^2 + 1\right]^{3.5}. \tag{25}$$

The nominator of equation (25) changes very rapidly with growing values of Z, while the denominator of equation (25) changes only slightly with increasing values of the rotation parameter. Therefore, the variation of the eddy viscosity in the near wall region of the rotating pipe is mainly influenced by the ratio of the Reynolds number based on the friction velocity. This is evident, because the shape of the velocity profiles close to the wall is dominated by viscous forces.

If $(\varepsilon_m^*)_0$ is known, the velocity distribution in the near wall region can be calculated from the identity

$$\frac{\mathrm{d}\tilde{v}_z}{\mathrm{d}y^+} = \frac{1 - y^+/\mathrm{Re}_*}{1 + \varepsilon_m^*}. \tag{26}$$

Because we are interested in this section to find only an approximation of the velocity profile close to the wall, the term y^+/Re_*, which appears in the nominator of equation (26), can be neglected in comparison to 1.

Reichhardt [9] performed many measurements concerning the distributions of the eddy viscosity and of the velocity profiles in a non-rotating pipe. He was able to develop an approximation for $(\varepsilon_m^*)_0$ for the region close to the wall. He stated that $(\varepsilon_m^*)_0$ in the near wall region ($y_0^+ < 30$) can be described according to

$$(\varepsilon_m^*)_0 = \kappa \left[y_0^+ - y_{10}^+ \arctan\left(\frac{y_0^+}{y_{10}^+}\right)\right] \tag{27}$$

where $y_0^+ = \tilde{y}(\mathrm{Re}_*)_0$ and $y_{10}^+ = 11$ is a constant. Rescaling equation (27) by using the wall coordinate y^+ for the rotating pipe flow according to equation (9) results in

$$(\varepsilon_m^*)_0 = \kappa \frac{(\mathrm{Re}_*)_0}{\mathrm{Re}_*} \left[y^+ - y_1^+ \arctan\left(\frac{y^+}{y_1^+}\right)\right] \tag{28}$$

with $y_1^+ = 11\ \mathrm{Re}_*/(\mathrm{Re}_*)_0$ according to Reichhardt [9]. Inserting equation (28) into equation (25) results in an approximation for the eddy viscosity in the near wall region.

$$\varepsilon_m^* = \left(\frac{\mathrm{Re}_*}{(\mathrm{Re}_*)_0}\right) \Big/ \left[\left(\frac{Z}{\mathrm{Re}_*}\right)^2 + 1\right]^{3.5} \kappa \left[y^+ - y_1^+ \arctan\left(\frac{y^+}{y_1^+}\right)\right]. \tag{29}$$

The distribution for ε_m^* given by equation (29) was found to be in good agreement with numerical calculations close to the wall ($y^+ \leq 30$). By using equation (29) an expression for $\tilde{v}_z$ for the near wall region can be obtained from equation (26) after integration

$$\tilde{v}_Z = \frac{1}{\kappa_1} \ln(1 + \kappa_1 y^+) + \int_0^{y^+} f(\xi)\, \mathrm{d}\xi \tag{30}$$

with the function $f(\xi)$ given by

$$f(\xi) = \frac{\kappa_1 y_1^+ \arctan(\xi/y_1^+)}{(1 + \kappa_1 \xi)\left[1 + \kappa_1 \xi - \kappa_1 y_1^+ \arctan(\xi/y_1^+)\right]}. \tag{31}$$

In the equations (30)–(31) the abbreviation

$$\kappa_1 = \kappa \left(\frac{\mathrm{Re}_*}{(\mathrm{Re}_*)_0}\right) \Big/ \left[\left(\frac{Z}{\mathrm{Re}_*}\right)^2 + 1\right]^{3.5} \tag{32}$$

was used. The integral, which appears in equation (30) cannot be solved analytically. Reichhard [9] derived an approximation for $f(\xi)$ in the case of non-rotating pipe flow. This function $f_1(\xi)$ can be used after some modifications to approximate $f(\xi)$ appearing in equation (30).

$$f_1(\xi) = \frac{7.8}{y_{10}^+} \left(\exp\left(-\frac{\xi}{y_1^+}\right) + (b\xi - 1)\exp(-b\xi)\right) \tag{33}$$

with

$$b = 0.33 \left[\left(\frac{\mathrm{Re}_*}{(\mathrm{Re}_*)_0}\right) \Big/ \left[\left(\frac{Z}{\mathrm{Re}_*}\right)^2 + 1\right]^{3.5}\right]^{1/2}. \tag{34}$$

For $Z \to 0$ equations (33)–(34) approach the approximation given by Reichhard [9]. The function $f_1(\xi)$, given by equation (33), agrees well with equation (31) for $10000 \leq \mathrm{Re}_D \leq 10^6$ and $0 \leq Z \leq 200$. Inserting equation (33) into equation (30) and integrating the resulting expression results in a formula for the velocity profile

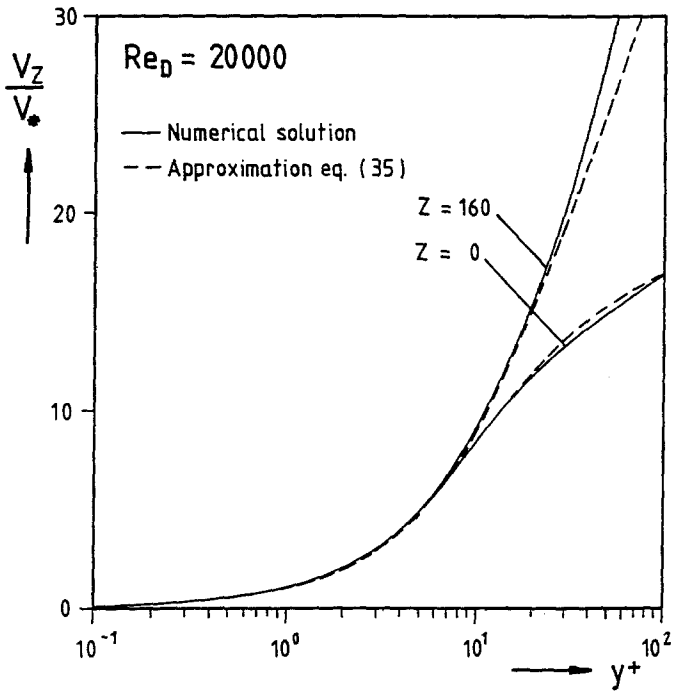

Fig. 10. Comparison between numerical solution and the approximation for v_Z/v_* in the near wall region.

in a rotating pipe in the near wall region

$$\tilde{v}_Z = \frac{1}{\kappa_1}\ln(1+\kappa_1 y^+) + 7.8\left[\frac{\mathrm{Re}_*}{(\mathrm{Re}_*)_0}\left(1-\exp\left(-\frac{y^+}{y_1^+}\right)\right) - \frac{y^+}{y_1^+}\exp(-by^+)\right]. \tag{35}$$

Figure 10 shows a comparison between the numerical solution of equation (11) and the approximation according to equation (35). It can be seen that the profiles coincide in the near wall region. For $y^+ > 30$ the profiles given by equation (35) deviate from the numerical solution. The velocity profiles according to equation (35) can be used in the future for numerical experiments as wall functions for the calculation of flows in rotating pipes and channels.

2.3. An Approximation Formula for the Whole Region of the Pipe

So far, we derived an expression for the axial velocity distribution in the core region and in the near wall region of the rotating pipe. For obtaining an approximation which is valid in the whole flow area, one has to combine the two expressions given by equation (15) and by equation (35). This can be done in the following way

$$\begin{aligned}\tilde{v}_Z = & \left\{ \frac{1}{\kappa_1} \ln(1 + \kappa_1 y^+) \right. \\ & \left. + 7.8 \left[\left(1 - \exp\left(-\frac{y^+}{y_1^+} \right) \right) \frac{\mathrm{Re}_*}{(\mathrm{Re}_*)_0} - \frac{y^+}{y_{10}^+} \exp(-by^+) \right] \right\} \\ & \times \{ \exp\left(-a_1(1 - \tilde{r})\right) \} + \left\{ \frac{v_{ZM}}{v_*} - A\tilde{r}B \right\} \\ & \times \{ 1 - \exp\left(-a_1(1 - \tilde{r})\right) \} \end{aligned} \tag{36}$$

with $a_1 = 5(\mathrm{Re}_*)_0/\mathrm{Re}_*$. It can be seen from equation (36) that the complete solution for $\tilde{v}_z$ consists of equation (15) and equation (35). The two velocity distributions are multiplied with the damping function $\exp\left(-a_1(1 - \tilde{r})\right)$, so that the velocity distribution in the near wall region dominates the velocity profile for small values of $\tilde{y}$, while the velocity distribution for the core region, equation (15), dominates the solution for increasing values of $\tilde{y}$. The term v_{ZM}/v_*, which appears in equation (36) is given graphically in Figure 8. However, using the continuity equation in integral form

$$\frac{\mathrm{Re}_D}{4\mathrm{Re}_*} = \int_0^1 \tilde{v}_z \tilde{r} \, \mathrm{d}\tilde{r} \tag{37}$$

and approximating the axial velocity distribution $\tilde{v}_z$ in equation (37) only by the expression for the core region, equation (15), results in the following simple expression for v_{ZM}/v_*.

$$\frac{v_{ZM}}{v_*} = \frac{\mathrm{Re}_D}{2\mathrm{Re}_*} + \frac{2A}{B+2} \tag{38}$$

where $A(Z)$ and $B(Z)$ are given by the equations (16)–(17). The values for v_{ZM}/v_* predicted from equation (38) are in good agreement with the numerical calculation shown in Figure 8. The maximum relative deviation between v_{ZM}/v_* given by equation (38) and the numerically predicted values was found to be approximately 5% for $10000 \leq \mathrm{Re}_D \leq 10^6$ and $0 \leq Z \leq 200$.

Figure 11 shows a comparison between the numerical solution of the conservation equation (11) and the approximation given by equation (36) for $\mathrm{Re}_D = 50000$ and $Z = 120$. Also the approximation for the velocity distribution in the core region and in the near wall region are plotted in the figure. It can be observed that the agreement between the approximation and the numerical calculation is good.

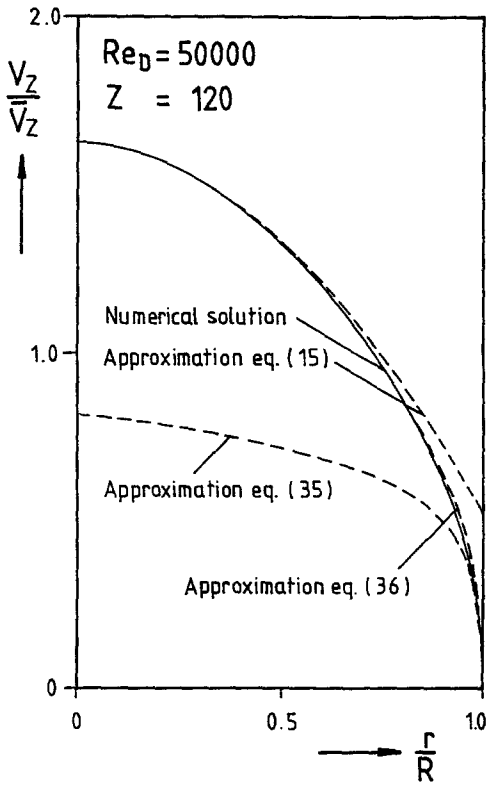

Fig. 11. Axial velocity distribution $v_Z/\bar{v}_Z$ for $\mathrm{Re}_D = 50000$ and $Z = 120$.

Only near the solid wall very small deviations between the approximation and the numerical solution can be observed.

Figure 12 elucidates the influence of the rotation parameter Z on the axial velocity distribution for two different flow-rate Reynolds numbers. It can be observed that increasing Z tends to relaminarize the flow. The axial velocity profiles tend to approach the parabolic distribution of the Hagen-Poiseuille flow for growing values of Z.

In Figure 13 approximately calculated velocity profiles according to equation (36) are compared with measurements of Reich [10]. As the approximative calculations nearly coincide with the numerical solution for $v_Z/\bar{v}_z$, only the profiles according to equation (36) have been plotted. It can be seen that the approximations are in good agreement with the measurements for various values of the parameter N and various values of the Reynolds number. Because in this plot the classical

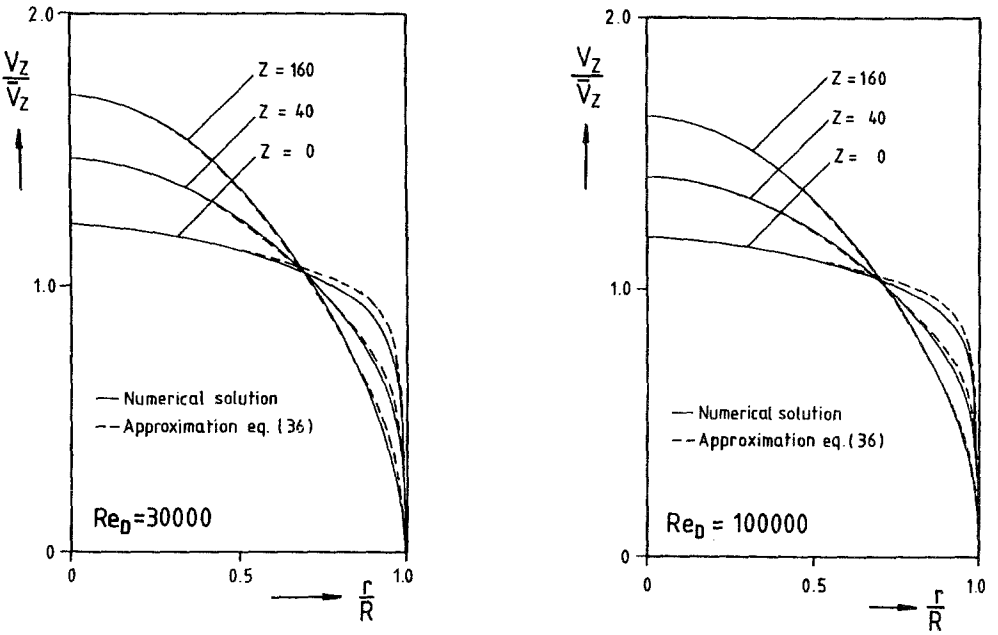

Fig. 12. Influence of a variation of the rotation parameter Z on the shape of the axial velocity profile.

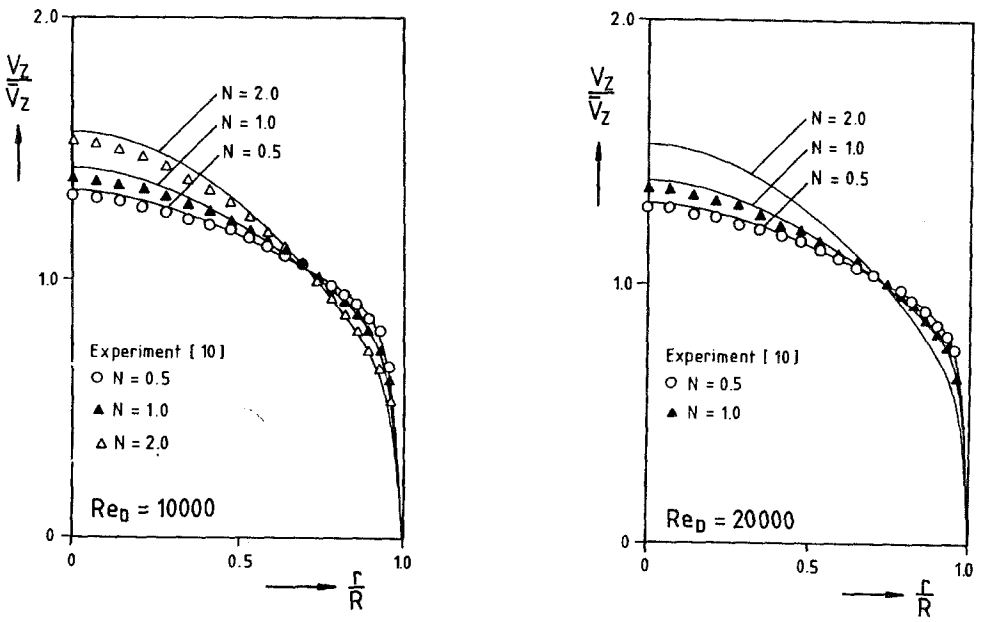

Fig. 13. Influence of a variation in N on the shape of the axial velocity profile.

rotation parameter N was used instead of Z, the agreement between measurements and approximation can be taken as a confirmation for the universal behavior of the velocity profiles in a rotating pipe.

3. Conclusions

According to the present investigation concerning the fully developed flow in an axially rotating pipe, the following major conclusions may be drawn:

- Using a modified rotation parameter Z instead of the classical parameter N, it was shown that universal axial velocity profiles exist in a rotating pipe.
- The velocity profiles close to the wall are mainly affected by the decreasing shear stress at the pipe wall due to pipe rotation.
- Wall functions could be developed for the axial velocity profile which take into account that the logarithmic region close to the wall disappears with growing rotation parameters Z.
- An approximation formula was developed for predicting the axial velocity profiles for the whole flow region. The approximation was found to be in good agreement with measurements of Reich [10].

As universal velocity profiles can be observed in turbulent rotating pipe flows, further experimental studies concerning this type of flows should use the rotation parameter Z instead of the classical parameter N for scaling the experimental results!

References

1. Borisenko, A.I., Kostikov, O.N. and Chumachenko, V.I., Experimental study of turbulent flow in a rotating channel. *J. Engng. Phys.* 24 (1973) 770–773.
2. Hirai, S. and Takagi, T., Prediction of heat transfer deterioration in turbulent swirling pipe flow. In: *Proc. 2nd ASME/JSME Thermal Engng. Joint Conf.* 5 (1987) pp. 181–187.
3. von Kármán, T., Über laminare und turbulente Reibung. *Z. Ang. Math. Mech.* 1 (1921) 233–251.
4. Kikuyama, K., Murakami, M., Nishibori, K. and Maeda, K., Flow in an axially rotating pipe. *Bull. JSME* 26 (1983) 506–513.
5. Koosinlin, M.L., Launder, B.E. and Sharma, B.I., Prediction of momentum, heat and mass transfer in swirling, turbulent boundary layers. *J. Heat Transfer* 96 (1975) 204–209.
6. F. Levy, Strömungserscheinungen in rotierenden Rohren. *VDI Forsch. Arb. Geb. Ing. Wes.* 322 (1929) 18–45.
7. Murakami, M. and Kikuyama, K., Turbulent flow in axially rotating pipes. *J. Fluids Engng.* 102 (1980) 97–103.
8. Lord Rayleigh, On the dynamics of revolving fluids. In: *Proc. R. Soc.* A93 (1917) pp. 148–154.
9. Reichhardt, H., Vollständige Darstellung der turbulenten Geschwindigkeitsverteilung in glatten Leitungen. *Z. Ang. Math. Mech.* 31 (1951) 208–219.
10. Reich, G. and Beer, H., Fluid flow and heat transfer in an axially rotating pipe – I. Effect of rotation on turbulent pipe flow. *Int. J. Heat Mass Transfer* 32 (1989) 551–562.
11. Schlichting, H., Grenzschicht-Theorie. Karlsruhe: G. Braun (1982).
12. Shchukin, V.K., Hydraulic resistance of rotating tubes. *J. Engng. Phys.* 12 (1967) 418–422.
13. Taylor, G.I., Stability of a viscous liquid contained between two rotating cylinders. *Phil. Trans. R. Soc. London* A223 (1923) 289–343.
14. Tietjens, O., Ströhmungslehre, Zweiter Band. Berlin/Heidelberg/New York: Springer (1970).
15. White, A., Flow of fluid in an axially rotating pipe. *J. Mech. Engng. Sci.* 6 (1964) 47–52.